Journal of Manufacturing Processes 79 (2022) 177–184

Contents lists available at ScienceDirect

Journal of Manufacturing Processes

journal homepage: www.elsevier.com/locate/manpro

Study of surface wettability on fused silica by ultrafast laser-induced micro/nano-surface structures☆

Kewei Li, Nathaniel Myers, Grant Bishop, Yuxin Li, Xin Zhao *

Department of Mechanical Engineering, Clemson University, Clemson, SC 29634-0921, USA

ARTICLE INFO

Keywords:
Ultrafast laser micromachining
Surface structuring
Surface wettability
Fused silica
Static contact angle
Surface roughness

ABSTRACT

Glass materials integrated with advanced functions, such as anti-fogging and self-cleaning functions, are urgently demanded in applications such as vehicle windshields, eyeglasses, goggles, electronic device screens, and windows. Inspired by nature, researchers have found multiscale surface structures to be a crucial factor in determining a material's surface wettability. The ultrafast pulsed laser is a promising tool to induce such surface structures and subsequently control the surface functionalities on different materials. The behavior of surface wettability with different micro/nano-scale surface structures created by femtosecond laser irradiation on fused silica is investigated in this research. The effects of laser fluence, overlapping ratio, and repetition rate on the structure morphology are studied. Seven different sorts of structures can be created by manipulating these parameters: (S1) micro-dots array, (S2) micro-dots array covered with laser-induced periodic surface structures (LIPSSs), (S3) LIPSSs, (S4) microgrooves covered with LIPSSs, (S5) microgrooves covered with irregular nanostructures, (S6) micro-channels and (S7) micro-channels covered with LIPSSs. Investigations into the static contact angle show that hydrophilic and superhydrophilic surfaces can be generated through the introduction of these laser-induced hierarchical structures. The relationship between laser parameters, surface structures, surface roughness, and surface wettability is established. Different distinctive mean static contact angle values are identified for different surface structures.

1. Introduction

The demands of anti-fogging and self-cleaning glass for applications such as eyeglasses, glass panels, and glass windows are rapidly increasing. To achieve such surface wettability-controlled functionalities, modifications on surface morphology/roughness [1] and chemical properties are required. Through applying additive coating [2–5] to change surface chemical properties, researchers have successfully prepared such surface functions on glass. However, such coating film is delicate and easy to be damaged in daily use. Fabricating multiscale structures on desired surfaces, inspired by functioning biological surfaces in nature such as lotus leaves [6], fly eyes [7], and fish skins [8], provides a robust alternative option for researchers.

In recent decades, ultrafast laser micromachining has become a research area of intense focus due to its ability to process practically any solid material such as metals, semiconductors, and dielectrics in a single step with extreme precision and great efficiency [9–13]. Ultrafast laser fabrication processes have been shown to generate a variety of surface morphologies with multiscale surface structures, which present unique surface functionalities without the requirement of post-process treatments [14–16]. Of particular interest of these surface morphologies are laser-induced periodic surface structures (LIPSSs), which are self-organized regularly recurring nanoripples formed on surfaces irradiated by linearly polarized radiation [16,17]. LIPSSs have emerged as an attractive phenomenon due to their ability to create functionalized surfaces for use in a variety of industrial, commercial, and military applications [18]. LIPSSs can be constructed to mimic a series of functional surfaces observed in nature including those with altered wettability [19–26], optical [26–29], and tribological [30–36] properties which result from the combination of micro/nanoscale surface structures.

So far, some experimental efforts have demonstrated the attainability of these wettability-controlled glass surfaces on fused silica [37–43], soda-lime glass [44,45], Borosilicate glass [46–48], and Zr-based bulk metallic glass [16] processed by ultrafast lasers. The majority of ultrafast laser processed glass surfaces display hydrophilicity and superhydrophilicity. By combining with post-processing like

☆ 50th SME North American Manufacturing Research Conference (NAMRC 50, 2022).

* Corresponding author.
E-mail address: xzhao5@clemson.edu (X. Zhao).

https://doi.org/10.1016/j.jmapro.2022.04.035
Received 12 April 2022; Accepted 23 April 2022

chemical processing, superhydrophobic surfaces can be achieved. For instance, He et al. [37] fabricated hexagonal micro-dots array through femtosecond laser irradiation and achieved superhydrophobic surface with silanization process. Dinh et al. [44] proposed one direct laser patterning technique to obtain a superhydrophobic surface with good transparency through the post-heating process. However, the relationship between ultrafast laser-induced surface structures, surface roughness, and surface wettability on fused silica has gotten little attention and is not well understood. A better understanding of the one-step ultrafast laser surface structuring technique on controlling the surface wettability of fused silica is needed. This study investigates the effects of laser fluence, overlapping ratio, repetition rate, and scanning strategy on the generated multiscale structural morphology and resultant wettability behaviors of fused silica. Wettability behavior can be readily understood by checking the surface roughness variation of created surface structures. The relationship between processing conditions, surface structures, surface roughness, and surface wettability will be established.

2. Experimental setup

2.1. Materials

All fused silica samples used in this study are Corning 7980, which is a typical high purity non-crystalline silica glass with excellent optical properties. Sample surfaces were well polished (60-40 scratch-dig based on MIL-PRF-13830B) and then subject to laser scanning. Before laser irradiation and characterization, all samples were cleaned in an ultrasonic washer for 5 min with isopropyl alcohol (99.9% purity).

2.2. Laser scanning and characterization

Laser scanning was conducted by a Yb: KGW femtosecond laser system (PHAROS by Light Conversion). The experiment setup is shown in Fig. 1. A linearly polarized Gaussian-shaped laser beam with a pulse duration of 190 fs was focused on the sample surface by a laser scan head (intelliSCAN by SCANLAB) for the two-dimensional surface scanning. The laser central wavelength is 1030 nm, and the beam diameters ω_0 (at $1/e^2$ of the peak intensity) are 5 mm and 34 μm before and after focusing, respectively. The single-pulse ablation threshold fluence of fused silica is 3.72 J/cm^2 determined through Liu's method [49]. Areas of 8×8 mm were patterned on sample surfaces with the scanning strategy shown in Fig. 2. The values of pulse distance (d_p) and line distance (d_l) were set to be equal to achieve uniform scanning. For some cases, line distance was set to be larger than pulse distance to fabricate micro-channels. In addition, a second scan with the low laser fluence and high overlapping ratio was applied to create LIPSSs over microchannels. Peak laser fluence (F_0), repetition rate (f), overlapping ratio (φ), and line distance (d_l) were varied in a wide range to study their

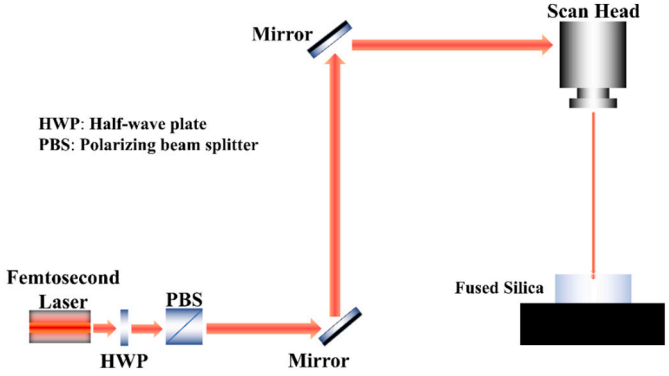

Fig. 1. Experimental setup.

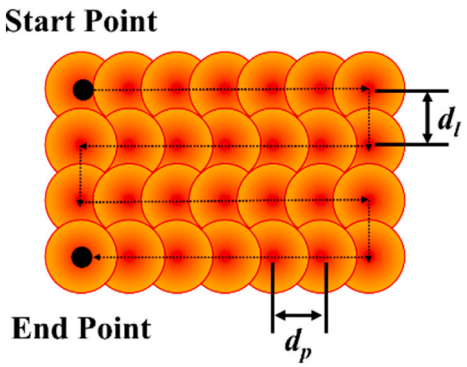

Fig. 2. Scanning strategy.

effects on surface structure formation and corresponding surface wettability variation, as summarized in Table 1. All experiments were conducted in an ambient atmosphere. The peak laser fluence F_0 is calculated as:

$$F_0 = \frac{8E_{pulse}}{\pi\omega_0{}^2}, \tag{1}$$

where E_{pulse} is the pulse energy. The overlapping ratio describes the ratio between the overlapped length of two consecutive pulses and spot diameters, which is defined as:

$$\varphi = \left(1 - \frac{v}{\omega_0 \times f}\right) \times 100\%, \tag{2}$$

where v is the scanning velocity.

After laser irradiation, the surface morphology of the processed sample was characterized through a scanning electron microscope (SEM) (Hitachi Regulus 8230). A 3D laser scanning microscope (Olympus LEXT OLS4100) was used to measure the roughness factor (r), which is defined as the ratio of the real surface area (A_r) over the projected surface area (A_p):

$$r = \frac{A_r}{A_p}. \tag{3}$$

The static contact angle was captured through a home-developed camera-based optical contact angle measurement system (shown in Fig. 3) at a constant room temperature around 25 °C and a constant humidity level of around 35%. The performance validation of this system has been conducted through a static contact angle measurement comparison with a commercial droplet shape analyzer (KRÜSS DSA10). The tested liquid was distilled water. The images of the water droplets were captured by the camera, and contact angles were measured by the ImageJ software [50].

Table 1
Laser parameters.

Uniform scanning	Repetition rate (kHz)	1, 10, 100
	Laser fluence (J/cm^2)	5, 10, 15, 20, 25, 30
	Scanning Speed (m/s)	(@10 kHz) 0.306, 0.272, 0.238, 0.204, 0.17, 0.136, 0.102, 0.068, 0.034, 0.017
	Line distance (μm)	(@10 kHz) 30.6, 27.2, 23.8, 20.4, 17, 13.6, 10.2, 6.8, 3.4, 1.7
Micro-channel	Repetition rate (kHz)	10
	Laser fluence (J/cm^2)	(First scan) 30; (second scan) 10
	Scanning speed (m/s)	(First scan) 0.017; (second scan) 0.102
	Line distance (μm)	(First scan) 35, 45, 60, 75, 90; (second scan) 10.2

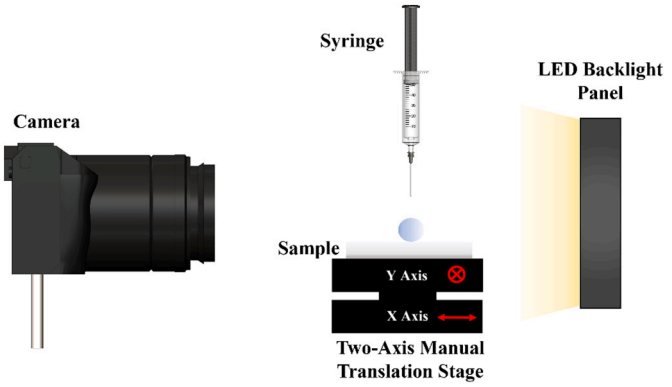

Fig. 3. Setup of the contact angle measurement system.

3. Results and discussions

3.1. Surface morphology

By varying laser fluence and overlapping ratio, five different types of surface structures were successfully obtained by uniform scanning, including: (a) micro-dots array, (b) micro-dots array with LIPSSs, (c) LIPSSs, (d) microgrooves with LIPSSs, and (f) microgrooves with irregular nanostructures (see Fig. 4). Higher magnification views of microgrooves with LIPSSs and microgrooves with irregular nanostructures are shown in Fig. 4(e) and (f). In Fig. 4(e), LIPSSs are observed on the surface of microgrooves generated. But for Fig. 4(f), as more energy is deposited at the same spot, microgrooves are split and scappled while LIPSSs are damaged and replaced by irregular nanostructures.

Fig. 5 summarizes the formation conditions of different surface structures through uniform scanning strategy, where S1–5 refer to micro-dots array, micro-dots array with LIPSSs, LIPSSs, microgrooves with LIPSSs, microgrooves with irregular nanostructures, respectively. Micro-channels (S6) and micro-channels with LIPSSs (S7) will be discussed later in this section. Different structures are observed in different overlapping ratio ranges. For micro-dots array (S1) (Fig. 4(a)), due to the low overlapping ratio, consecutive laser pulses do not overlap. Therefore, each micro-dot represents a single laser pulse ablation crater. When the scanning speed is reduced and the overlapping ratio is increased, these laser pulse ablation sites tend to partially overlap, triggering the formation of LIPSSs on top of the micro-dots, and the surface morphology is switched to micro-dots array with LIPSSs (S2) (Fig. 4(b)). Here, LIPSSs (S3) (Fig. 4(c)) are generated at the periphery areas of laser beam ablation sites. With an even higher overlapping ratio, LIPSSs expand towards the center of the laser ablation site, eventually encompassing the entire treated surface. No single laser ablation crater can be recognized due to the high overlapping ratio, and the third type of surface morphology, LIPSSs, is formed. LIPSSs on fused silica are parallel to the laser polarization direction, which is consistent with previous findings [51]. More energy is deposited to the same spot when the overlapping ratio is increased, stimulating the formation of microgrooves (S4). These microgrooves are covered by LIPSSs due to the scanning effect (Fig. 4(d) and (e)). When the overlapping ratio becomes extremely high (over 90%), microgrooves tend to split, and LIPSSs are replaced by irregular nanostructures (Fig. 4(f)).

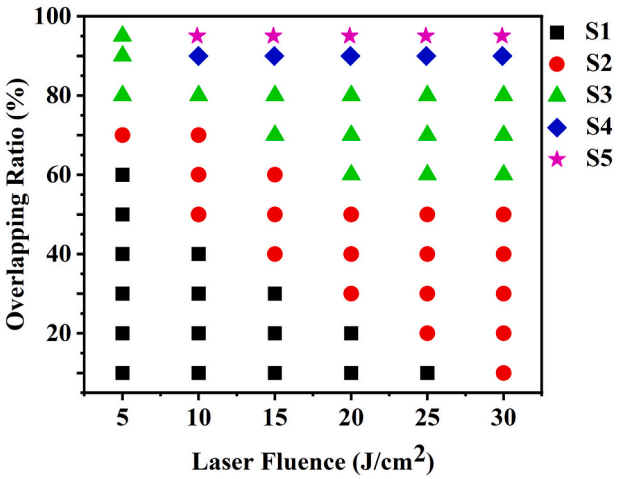

Fig. 5. Formation conditions for different types of surface structures. The repetition rate is 10 kHz. S1: micro-dots array, S2: micro-dots array with LIPSSs, S3: LIPSSs, S4: microgrooves with LIPSSs, and S5: microgrooves with irregular nanostructures.

Laser fluence has a significant impact on the creation of surface structures as well. The micro-dots array (with/without LIPSSs) is more likely to be created in low laser fluence circumstances due to the narrow beam diameter. At higher laser fluences with the same overlapping ratio,

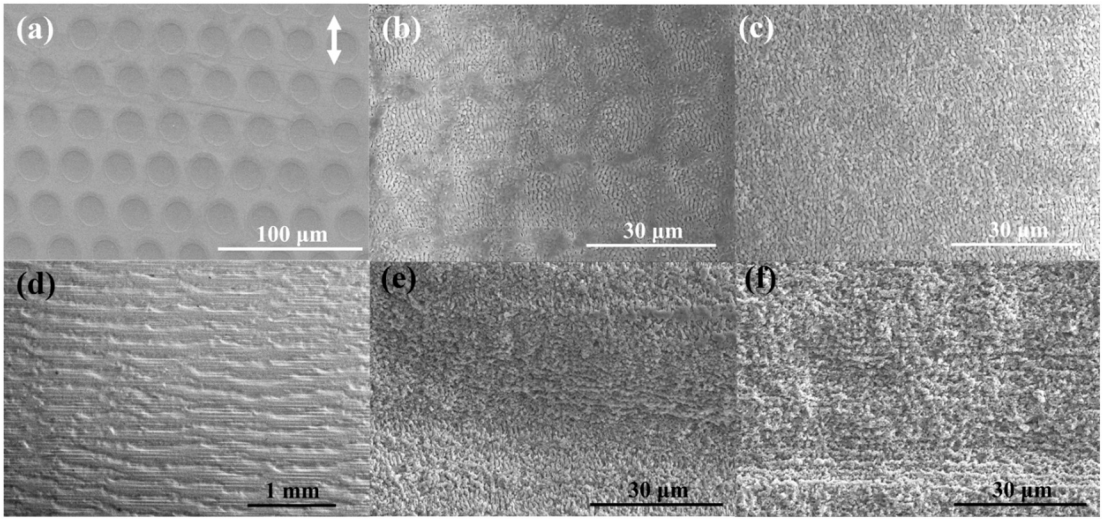

Fig. 4. SEM images of different obtained surface structures. (a): Micro-dots array, (b): micro-dots array with LIPSSs, (c): LIPSSs, (d): microgrooves with LIPSSs, (e): high magnification view of microgrooves with LIPSSs and (f): high magnification view of microgrooves with irregular nanostructures. The repetition rate is 10 kHz, and the laser fluence is 25 J/cm^2. The white double arrow indicates laser polarization direction.

the beam diameter becomes larger to induce large overlaps between consecutive pulses. Single craters will be eliminated and uniform LIPSSs will be created. With a 10% overlapping ratio, micro-dots array with LIPSSs could be obtained at the laser fluence of 30 J/cm^2. These micro-dots cannot be formed for the 5 J/cm^2 instance due to the low laser energy density, even with the greatest overlapping ratio (95%).

In addition to the structures mentioned above, micro-channels and micro-channels covered with LIPSSs were also successfully fabricated, as shown in Fig. 6. By applying a strong laser fluence of 30 J/cm^2 and various line distances described in Table 1, multiple parallel micro-channels were scribed on sample surfaces (Fig. 6(a) and (b)). To induce LIPSSs on their surfaces, these scribed microchannels were then subjected to a second cycle of laser scanning with a fluence of 10 J/cm^2 and an overlapping ratio of 70%. Micro-channels with LIPSSs were successfully obtained by this double scanning method (Fig. 6(c) and (d)).

Fig. 6(a) and (c) shows low magnification SEM images of micro-channels with and without LIPSSs, respectively. Without the second scanning, the area between micro-channels is flat and smooth. By introducing the second uniform scanning, LIPSSs are generated in the whole processed area and visible in the space between those micro-channels. In Fig. 6(b) and (d) which display high magnification views of micro-channels and micro-channels with LIPSSs, LIPSSs are clearly found to be formed on the bottom of micro-channels (Fig. 6(b)) and the blank area between micro-channels (Fig. 6(d)).

3.2. Surface wettability

The static contact angle is a widely used parameter indicating the performance of surface wettability which is captured when liquid droplet is in a static stable state. In this paper, surface wettability was mainly identified and analyzed by this contact angle. The unprocessed fused silica sample (Fig. 7(a)) is hydrophilic, with a contact angle of around 47°. Fig. 7(b–d) shows the wettability transition behavior of laser processed fused silica from hydrophilicity to superhydrophilicity with the generation of the micro-dots array, LIPSSs, and microgrooves with LIPSSs. Fig. 8(a) summarizes the relationship between the contact angle, laser fluence, and overlapping ratio. It is observed that all surface structures help reduce contact angle, and at some conditions, the surface wettability can be changed from hydrophilicity to superhydrophilicity. For example, the contact angle is reduced to below 2° by inducing microgrooves, which satisfies the anti-fogging requirement (<5°). Such behavior could be explained through Wenzel's model [52,53]. In this model, a liquid droplet is regarded as fully attached to the processed surface and no space left between the liquid and surface. The contact angle of the roughened surface (θ_r) is described by:

$$cos(\theta_r) = rcos(\theta_0), \tag{4}$$

where r is the roughness factor which is the ratio between the real surface area and projected surface area, and θ_0 is the intrinsic contact angle on the original flat surface. Since the fused silica is intrinsically hydrophilic to water ($\theta_0 \approx 47°$) the surface roughness will always decrease the contact angle as r is always larger than 1. Changing surface chemical characteristics, such as providing a hydrophobic coating, could be one method for reversing the trend.

The effects of laser fluence and overlapping ratio can be clearly revealed by Fig. 8(a). To better understand the mechanism, the corresponding surface roughness factors at different conditions are summarized in Fig. 8(b). Note that the contact angle and surface roughness of untreated fused silica are shown as the case with a 0 overlapping ratio in Fig. 8(a) and (b), respectively. It is found that at the same laser fluence, the contact angle decreases with the increase of the overlapping ratio. As the overlapping ratio increases, the created surface structures could switch from micro-dots array to LIPSSs, and finally to microgrooves, as illustrated in Fig. 5. This surface structure transition results in an increase of surface roughness factor, as shown in Fig. 8(b) and hence a lower contact angle.

The surface wettability is also influenced by the laser fluence. As the laser fluence increases, the contact angle generally decreases with the same overlapping ratio. This phenomenon is also attributed to the transition of created surface structures and the resultant roughness factor increase. As shown in Fig. 5, it is easier to produce surface structures with higher roughness factors, like microgrooves, with a higher laser fluence. Therefore, a higher laser fluence usually leads to a lower contact angle, supported by the surface roughness factor results in Fig. 8(b). However, the case with the laser fluence of 30 J/cm^2 is an

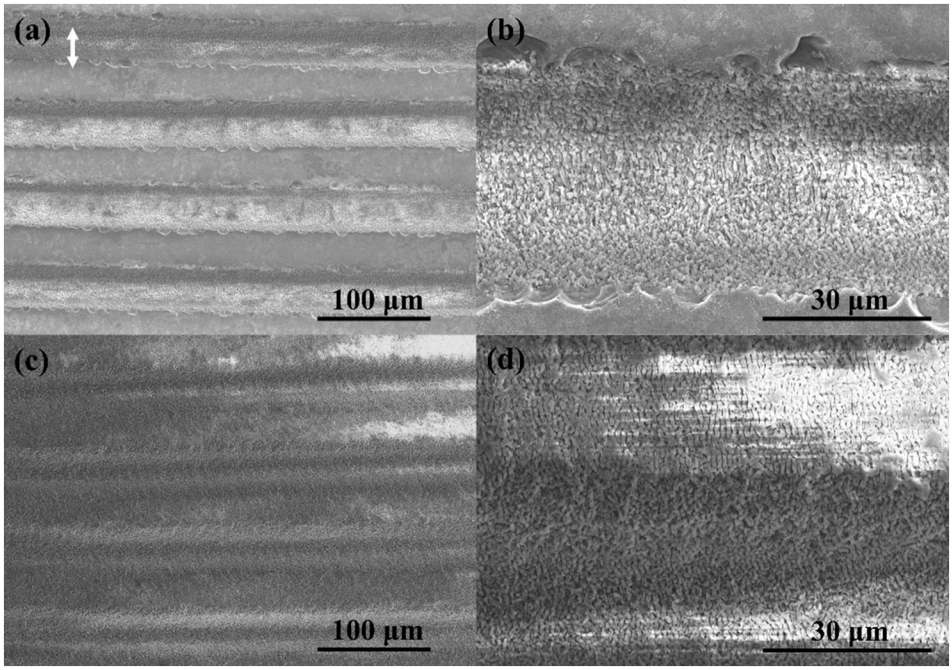

Fig. 6. Surface morphology of (a) micro-channels with (b) its high magnification view and (c) micro-channels with LIPSSs with (d) its higher magnification view. The repetition rate is 10 kHz.

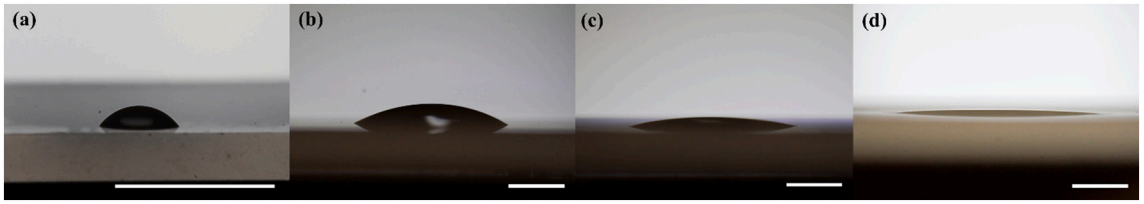

Fig. 7. Surface wettability of (a) unprocessed surface, (b) micro-dots array, (c) LIPSSs and (d) microgrooves with LIPSSs. The length of the scale bar corresponds to 2 mm.

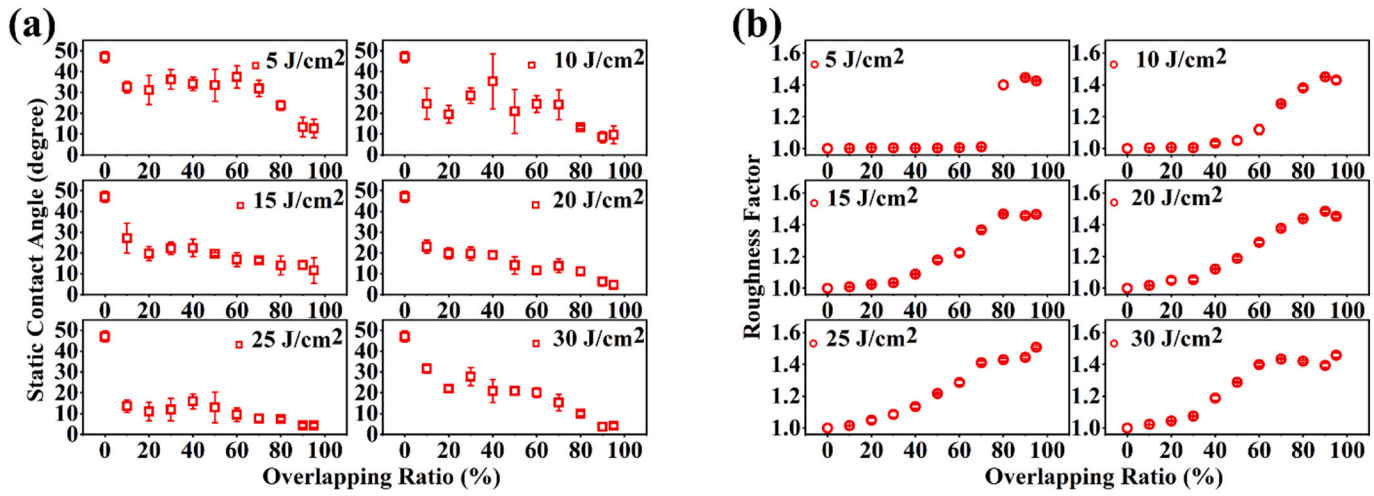

Fig. 8. (a) Static contact angle results and (b) roughness factor results obtained with different laser fluences and overlapping ratios. The repetition rate is 10 kHz.

exception. The contact angle for this instance is much higher than that for the case of 20 J/cm^2, although its roughness factor is still slightly higher. It is hypothesized that this phenomenon might be caused by the surface chemistry change during the intense laser ablation at a high laser fluence, which should be further studied by the future research.

Laser pulse repetition rate is another important factor in ultrafast laser processing. The contact angles achieved at different repetition rates (1 kHz, 10 kHz, and 100 kHz) and overlapping ratios at the same laser fluence are summarized in Fig. 9. Statistically, the contact angle is less sensitive to the repetition rate. This observation is consistent with the finding in [54] that the repetition rate has a minor influence on surface morphology.

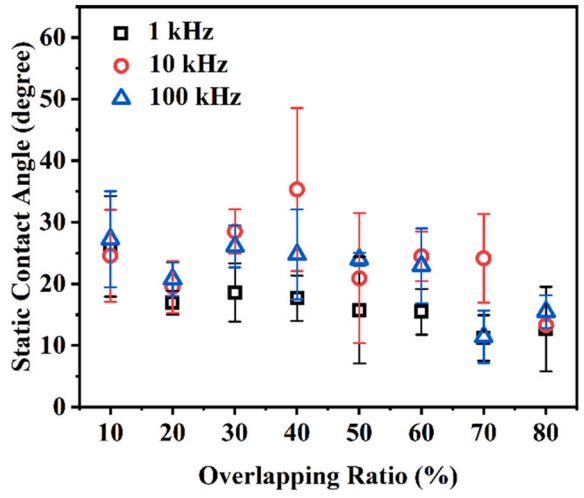

Fig. 9. Static contact angle results obtained with different repetition rates. Laser fluence is 10 J/cm^2.

Apart from uniform scanning results, measurement of static contact angle on samples containing micro-channels was also carried out and shown in Fig. 10(a). When the line distance between micro-channels is increased to 75 μm, the static contact angle stays less than 19°, and the surface has excellent water affinity. In addition, a V-shape tendency is noted, with the lowest contact angle value at 45 μm. When the line distance increases from 45 to 90 μm, the performance of super-hydrophilicity diminishes slightly. Such unusual behavior could be attributed to the reduction of surface roughness. As the line distance increases, the actual processed area within the whole laser projected area decreases, which helps reduce the overall surface roughness and drive surface wettability back towards the pristine state. Furthermore, the case with a line distance equal to 45 μm exhibits the lowest mean contact angle value which can be explained through roughness factor measurement shown in Fig. 10(b). Because the 45 μm case has the highest roughness factor, the contact angle tested is expected to be the lowest compared with the other cases. When the line distance rises, with decreasing roughness factor, the contact angle increases according to Eq. (4). In addition, the introduction of LIPSSs generally shows an enhancing effect on superhydrophilicity. By applying the second scan with a lower laser fluence and scanning speed to create LIPSSs, the contact angle is smaller than that obtained from a single scan due to the enhancement of surface roughness observed in Fig. 10(b).

To further elucidate the relationship between surface wettability and surface structures, contact angle results of each surface structure including all corresponding processing parameters are summarized in Fig. 11(a). Here, surface structures number was assigned to each surface morphology: (S1) micro-dots array, (S2) micro-dots array with LIPSSs, (S3) LIPSSs, (S4) microgrooves with LIPSSs, (S5) microgrooves with irregular nanostructures, (S6) micro-channels and (S7) micro-channels with LIPSSs. Although there is overlapping in contact angle values among generated surface structures, each surface structure has its own characteristic (mean) contact angle range. Microgrooves (S4, S5) offer

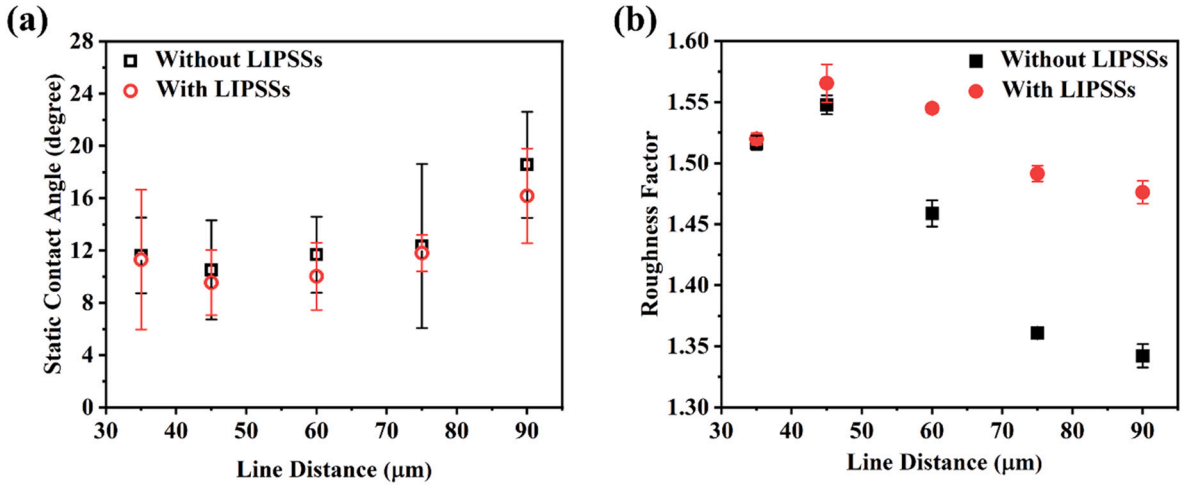

Fig. 10. (a) Static contact angle results and (b) roughness factor results obtained from micro-channels cases. The repetition rate is 10 kHz.

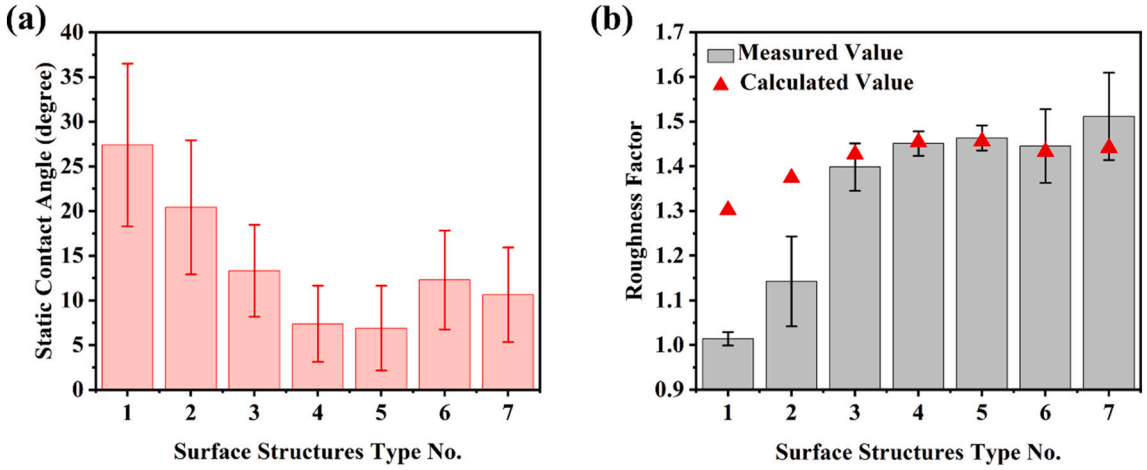

Fig. 11. (a) Static contact angle results of different surface morphologies and (b) experimentally measured and theoretically calculated roughness factors of different surface structures.

the lowest static contact angle in general. The effect of LIPSSs (S3) on surface wettability is discernible and confirmed again. By adding LIPSSs on other structures (micro-dots and micro-channels), the contact angle decreases.

Fig. 11(b) summarizes the measured roughness factor of various surface structures. The theoretically calculated values based on Eq. (4) are also displayed as a comparison. These theoretical roughness factors are calculated based on the mean contact angle values shown in Fig. 11 (a). In general, measurements and calculations correspond well, demonstrating that Wenzel's model can adequately explain the wettability variation caused by varied surface structures. Larger disparities are seen in the situations of micro-dots array and micro-dots array with LIPSSs, and the real surface roughness is smaller than the theoretical value to generate such low contact angle. There might be another phenomenon such as surface chemical property changes involved during the laser scanning process.

4. Conclusion

Ultrafast laser-induced micro-/nano-surface structure formation and corresponding surface wettability are studied in the paper. The effects of laser fluence, overlapping ratio, repetition rate, and scanning strategies are investigated on fused silica. Seven types of surface structures are obtained: (S1) micro-dots array, (S2) micro-dots array with LIPSSs, (S3) LIPSSs, (S4) microgrooves with LIPSSs, (S5) microgrooves with irregular nanostructures, (S6) micro-channels, and (S7) micro-channels with LIPSSs. It is found that surface structuring could reduce the water contact angle on fused silica surfaces. They could be changed from hydrophilic to superhydrophilic surfaces by forming microgrooves. The addition of surface roughness by adding LIPSSs has also been proven to assist the reduction of the contact angle. The static contact angle decreases with increased laser fluence and overlapping ratio, due to the surface structure transition and the resultant surface roughness increase, which is consistent with the Wenzel's model. The clear relationship among laser processing parameters, surface morphology, surface roughness, and surface wettability for fused silica, which was missed, is established. The revealed relationship provides a guideline for wettability control of fused silica using ultrafast laser surface structuring and could enable its applications in microfluidics, windows, electronics, automobiles, safety goggles, etc.

Declaration of competing interest

The authors declare that they have no known competing financial interests or personal relationships that could have appeared to influence the work reported in this paper.

Acknowledgements

The authors would like to gratefully acknowledge the financial support provided for this study by the National Science Foundation (Grant No: 2047000-CMMI). The authors thank Clemson University Electron Microscopy Facility and Clemson Light Imaging Facility for the access to scanning electron microscopy and optical microscopy equipment. The authors also would like to thank Dr. Konstantin Kornev from the Department of Materials Science and Engineering at Clemson University for the access to their droplet shape analyzer (KRÜSS DSA10) for the performance validation of our self-developed contact angle system.

References

[1] AlRatrout A, Blunt MJ, Bijeljic B. Wettability in complex porous materials, the mixed-wet state, and its relationship to surface roughness. Proc. Natl. Acad. Sci. U. S. A. 2018;115:8901–6. https://doi.org/10.1073/pnas.1803734115.
[2] Wang Y, Zhu Y, Zhang C, Li J, Guan Z. Transparent, superhydrophobic surface with varied surface tension responsiveness in wettability based on tunable porous silica structure for gauging liquid surface tension. ACS Appl. Mater. Interfaces 2017;9:4142–50. https://doi.org/10.1021/acsami.6b12779.
[3] Si Y, Zhu H, Chen L, Jiang T, Guo Z. A multifunctional transparent superhydrophobic gel nanocoating with self-healing properties. Chem. Commun. 2015;51:16794–7. https://doi.org/10.1039/c5cc06977g.
[4] Zhao S, Zhao J, Wen M, Yao M, Wang F, Huang F, et al. Sequentially reinforced additive coating for transparent and durable superhydrophobic glass. Langmuir 2018;34:11316–24. https://doi.org/10.1021/acs.langmuir.8b01960.
[5] Ling XY, Phang IY, Vancso GJ, Huskens J, Reinhoudt DN. Stable and transparent superhydrophobic nanoparticle films. Langmuir 2009;25:3260–3. https://doi.org/10.1021/la8040715.
[6] Feng L, Li S, Li Y, Li H, Zhang L, Zhai J, et al. Super-hydrophobic surfaces: from natural to artificial. Adv. Mater. 2002;14:1857–60. https://doi.org/10.1002/adma.200290020.
[7] Sun Z, Liao T, Liu K, Jiang L, Kim JH, Dou SX. Fly-eye inspired superhydrophobic anti-fogging inorganic nanostructures. Small 2014;10:3001–6. https://doi.org/10.1002/smll.201400516.
[8] Liu M, Wang S, Wei Z, Song Y, Jiang L. Bioinspired design of a superoleophobic and low adhesive water/solid interface. Adv. Mater. 2009;21:665–9. https://doi.org/10.1002/adma.200801782.
[9] Ahmmed K, Grambow C, Kietzig A-M. Fabrication of micro/nano structures on metals by femtosecond laser micromachining. Micromachines 2014;5:1219–53. https://doi.org/10.3390/mi5041219.
[10] Cerami L, Mazur E, Nolte S, Schaffer CB. Femtosecond laser micromachining. In: Thomson R, Leburn C, Reid D, editors. Ultrafast Nonlinear Opt. Heidelberg: Springer International Publishing; 2013. p. 287–321. https://doi.org/10.1007/978-3-319-00017-6_12.
[11] Mannion P, Magee J, Coyne E, O'Connor GM. Ablation thresholds in ultrafast laser micromachining of common metals in air. In: Glynn TJ, editor. Proc. SPIE. vol. 4876; 2003. p. 470. https://doi.org/10.1117/12.463744.
[12] Meunier M, Fisette B, Houle A, Kabashin AV, Broude SV, Miller P. Processing of metals and semiconductors by a femtosecond laser-based microfabrication system. In: Neev J, Ostendorf A, Schaffer CB, editors. Proc. SPIE. vol. 4978; 2003. p. 169. https://doi.org/10.1117/12.478595.
[13] Gattass RR, Mazur E. Femtosecond laser micromachining in transparent materials. Nat. Photonics 2008;2:219–25. https://doi.org/10.1038/nphoton.2008.47.
[14] Bonse J, Hohm S, Kirner SV, Rosenfeld A, Kruger J. Laser-induced periodic surface structures—a scientific evergreen. IEEE J. Sel. Top Quantum Electron. 2017;23:1. https://doi.org/10.1109/JSTQE.2016.2614183.
[15] Fan P, Pan R, Zhong M. Ultrafast laser enabling hierarchical structures for versatile superhydrophobicity with enhanced Cassie–Baxter stability and durability. Langmuir 2019;35:16693–711. https://doi.org/10.1021/acs.langmuir.9b02986.
[16] Jiao Y, Brousseau E, Shen X, Wang X, Han Q, Zhu H, et al. Investigations in the fabrication of surface patterns for wettability modification on a Zr-based bulk metallic glass by nanosecond laser surface texturing. J. Mater. Process. Technol. 2020;283:116714. https://doi.org/10.1016/j.jmatprotec.2020.116714.
[17] Bonse J, Krüger J, Höhm S, Rosenfeld A. Femtosecond laser-induced periodic surface structures. J. Laser Appl. 2012;24:042006. https://doi.org/10.2351/1.4712658.
[18] Bonse J, Kirner SV, Höhm S, Epperlein N, Spaltmann D, Rosenfeld A, et al. Applications of laser-induced periodic surface structures (LIPSS). In: Klotzbach U, Washio K, Kling R, editors. Proc. SPIE. vol. 10092; 2017. 100920N. https://doi.org/10.1117/12.2250919.
[19] Lee HJ, Michielsen S. Lotus effect: superhydrophobicity. J. Text. Inst. 2006;97:455–62. https://doi.org/10.1533/joti.2006.0271.
[20] Patankar NA. Mimicking the lotus effect: influence of double roughness structures and slender pillars. Langmuir 2004;20:8209–13. https://doi.org/10.1021/la048629t.
[21] Lu J, Ngo C-V, Singh SC, Yang J, Xin W, Yu Z, et al. Bioinspired hierarchical surfaces fabricated by femtosecond laser and hydrothermal method for water harvesting. Langmuir 2019;35:3562–7. https://doi.org/10.1021/acs.langmuir.8b04295.
[22] Wu J, Yin K, Xiao S, Wu Z, Zhu Z, Duan J-A, et al. Laser fabrication of bioinspired gradient surfaces for wettability applications. Adv. Mater. Interfaces 2021;8:2001610. https://doi.org/10.1002/admi.202001610.
[23] Wu B, Zhou M, Li J, Ye X, Li G, Cai L. Superhydrophobic surfaces fabricated by microstructuring of stainless steel using a femtosecond laser. Appl. Surf. Sci. 2009;256:61–6. https://doi.org/10.1016/j.apsusc.2009.07.061.
[24] Li J, Zhou Y, Fan F, Du F, Yu H. Controlling surface wettability and adhesive properties by laser marking approach. Opt. Laser Technol. 2019;115:160–5. https://doi.org/10.1016/j.optlastec.2019.02.023.
[25] Cheng H-C, Jiang Z-X, Chang T-L, Chen P-H. Roughness and wettability properties of plain and silica-coated copper surfaces textured with picosecond laser. Appl. Surf. Sci. 2020;514:145918. https://doi.org/10.1016/j.apsusc.2020.145918.
[26] Smith GS. Structural color of Morpho butterflies. Am. J. Phys. 2009;77:1010–9. https://doi.org/10.1119/1.3192768.
[27] Zhao Y, Xie Z, Gu H, Zhu C, Gu Z. Bio-inspired variable structural color materials. Chem. Soc. Rev. 2012;41:3297. https://doi.org/10.1039/c2cs15267c.
[28] Gu Z-Z, Uetsuka H, Takahashi K, Nakajima R, Onishi H, Fujishima A, et al. Structural color and the lotus effect. Angew. Chem. Int. Ed. 2003;42:894–7. https://doi.org/10.1002/anie.200390235.
[29] Wu P, Cao X, Zhao L, Chen Z, Zhang M, Juodkazis S, et al. Dynamic structural color display based on femtosecond laser variable polarization processing. Adv. Mater. Interfaces 2021;8:2100460. https://doi.org/10.1002/admi.202100460.
[30] Müller F, Kunz C, Gräf S. Bio-inspired functional surfaces based on laser-induced periodic surface structures. Materials (Basel) 2016;9:476. https://doi.org/10.3390/ma9060476.
[31] Klein M-CG, Gorb SN. Epidermis architecture and material properties of the skin of four snake species. J. R. Soc. Interface 2012;9:3140–55. https://doi.org/10.1098/rsif.2012.0479.
[32] Hazel J, Stone M, Grace M, Tsukruk V. Nanoscale design of snake skin for reptation locomotions via friction anisotropy. J. Biomech. 1999;32:477–84. https://doi.org/10.1016/S0021-9290(99)00013-5.
[33] Eichstät J, Römer GRBE, Huis in't Veld AJ. Towards friction control using laser-induced periodic Surface Structures. Phys. Procedia 2011;12:7–15. https://doi.org/10.1016/j.phpro.2011.03.099.
[34] Bonse J, Kirner S, Griepentrog M, Spaltmann D, Krüger J. Femtosecond laser texturing of surfaces for tribological applications. Materials (Basel) 2018;11:801. https://doi.org/10.3390/ma11050801.
[35] Bonse J, Koter R, Hartelt M, Spaltmann D, Pentzien S, Höhm S, et al. Tribological performance of femtosecond laser-induced periodic surface structures on titanium and a high toughness bearing steel. Appl. Surf. Sci. 2015;336:21–7. https://doi.org/10.1016/j.apsusc.2014.08.111.
[36] Bonse J, Koter R, Hartelt M, Spaltmann D, Pentzien S, Höhm S, et al. Femtosecond laser-induced periodic surface structures on steel and titanium alloy for tribological applications. Appl. Phys. A Mater. Sci. Process. 2014;117:103–10. https://doi.org/10.1007/s00339-014-8229-2.
[37] He X, Li G, Zhang Y, Lai X, Zhou M, Xiao L, et al. Bioinspired functional glass integrated with multiplex repellency ability from laser-patterned hexagonal texturing. Chem. Eng. J. 2021;416:129113. https://doi.org/10.1016/j.cej.2021.129113.
[38] Deng C, Ki H. Tunable wetting surfaces with interacting cavities via femtosecond laser patterning and wet etching. J. Appl. Phys. 2020;128:015306. https://doi.org/10.1063/5.0011885.
[39] Lin Y, Han J, Cai M, Liu W, Luo X, Zhang H, et al. Durable and robust transparent superhydrophobic glass surfaces fabricated by a femtosecond laser with exceptional water repellency and thermostability. J. Mater. Chem. A 2018;6:9049–56. https://doi.org/10.1039/C8TA01965G.
[40] Stroj S, Kasemann S, Domke M, Piredda G, Zehetner J, Matylitskaya V. Transparent superhydrophobic surfaces with high adhesion generated by the combination of femtosecond laser structuring and wet oxidation. Appl. Surf. Sci. 2017;420:550–7. https://doi.org/10.1016/j.apsusc.2017.05.045.
[41] Xu S-zhen, Dou H qiang, Sun K, Ye Y yun, Li Z, Wang H jun, et al. Scan speed and fluence effects in femtosecond laser induced micro/nano-structures on the surface of fused silica. J. Non-Cryst. Solids 2018;492:56–62. https://doi.org/10.1016/j.jnoncrysol.2018.04.018.
[42] Kunz C, Müller FA, Gräf S. Multifunctional hierarchical surface structures by femtosecond laser processing. Materials (Basel) 2018;11. https://doi.org/10.3390/ma11050789.
[43] Kunz C, Engel S, Müller F, Gräf S. Large-area fabrication of laser-induced periodic surface structures on fused silica using thin gold layers. Nanomaterials 2020;10:1187. https://doi.org/10.3390/nano10061187.
[44] Dinh T-H, Ngo C-V, Chun D-M. Direct laser patterning for transparent superhydrophobic glass surfaces without any chemical coatings. Appl. Phys. A Mater. Sci. Process. 2020;126:462. https://doi.org/10.1007/s00339-020-03653-9.
[45] Soldera M, Alamri S, Sürmann PA, Kunze T, Lasagni AF. Microfabrication and surface functionalization of soda lime glass through direct laser interference patterning. Nanomaterials 2021;11:129. https://doi.org/10.3390/nano11010129.
[46] Zhou M, Yang HF, Li BJ, Dai J, Di JK, Zhao EL, et al. Forming mechanisms and wettability of double-scale structures fabricated by femtosecond laser. Appl. Phys. A Mater. Sci. Process. 2009;94:571–6. https://doi.org/10.1007/s00339-008-4920-5.
[47] Wang Z, Nandyala D, Colosqui CE, Cubaud T, Hwang DJ. Glass surface micromachining with simultaneous nanomaterial deposition by picosecond laser for wettability control. Appl. Surf. Sci. 2021;546:149050. https://doi.org/10.1016/j.apsusc.2021.149050.

[48] Lee D-K, Cho YH, Lee JW, Park MS. Wettability of microstructured Pyrex glass with hydrophobic and hydrophilic properties. Surf. Coat. Technol. 2017;319:213–8. https://doi.org/10.1016/j.surfcoat.2017.04.022.
[49] Liu JM. Simple technique for measurements of pulsed Gaussian-beam spot sizes. Opt. Lett. 1982;7:196. https://doi.org/10.1364/OL.7.000196.
[50] https://imagej.nih.gov/ij/.
[51] Höhm S, Rosenfeld A, Krüger J, Bonse J. Femtosecond diffraction dynamics of laser-induced periodic surface structures on fused silica. Appl. Phys. Lett. 2013; 102. https://doi.org/10.1063/1.4790284.
[52] Wenzel RN. Resistance of solid surfaces to wetting by water. Ind. Eng. Chem. 1936; 28:988–94. https://doi.org/10.1021/ie50320a024.
[53] Wenzel RN. Surface roughness and contact angle. J. Phys. Colloid Chem. 1949;53: 1466–7. https://doi.org/10.1021/j150474a015.
[54] Li K, Zhao X. Formation of micro-/nano-surface structures on stainless steel by ultrafast lasers. In: Process. Mater. Vol. 2. American Society of Mechanical Engineers; 2019. https://doi.org/10.1115/MSEC2019-3023.